Solar forced diurnal regulation of cave drip rates via phreatophyte evapotranspiration

Katie Coleborn[1], Gabriel C. Rau[1], Mark O. Cuthbert [2], Andy Baker[1], Owen Navarre[3]

[1]*Connected Waters Initiative Research Centre, UNSW Australia, Kensington, NSW 2052 Australia*

[2]*School of Geography, Earth and Environmental Sciences, University of Birmingham, Edgbaston, Birmingham, B15 2TT, UK*

[3]*School of Biology Earth and Environmental Sciences, UNSW Australia, Kensington, NSW 2052 Australia*

Corresponding author: Katie Coleborn

Email: k.coleborn@unsw.edu.au

Tel: +61434105636

Abstract

We present results of a detailed study of drip rate variations at 12 drip discharge sites in Glory Hole Cave, New South Wales, Australia. Our novel time series analysis, using the synchrosqueeze transform, reveals pronounced oscillations at daily and sub-daily frequencies occurring in 8 out of the 12 monitored sites. These oscillations were not spatially or temporally homogenous, with different drip sites exhibiting such behaviour at different times of year in different parts of the cave. We test several hypotheses for the cause of the oscillations including variations in pressure gradients between karst and cave due to cave breathing effects or atmospheric and earth tides, variations in hydraulic conductivity due to changes in viscosity of water with daily temperature oscillations, and solar driven daily cycles of vegetative (phreatophytic) transpiration. We conclude that the only hypothesis consistent with the data and hydrologic theory is that daily oscillations are caused by solar driven pumping by phreatophytic trees which are abundant at the site. The daily oscillations are not continuous and occur sporadically in short bursts (2-14 days) throughout the year due to non-linear modification of the solar signal via complex karst architecture. This is the first observation of tree water use in cave drip water and has important implications for karst hydrology in regards to developing a new protocol to determine the relative importance of trends in drip rate, such as diurnal oscillations, and how these trends change over timescales of weeks to years. This information can be used to infer karst architecture. This study also demonstrates the importance of vegetation on recharge dynamics, information that will inform both process-based karst models and empirical estimation approaches. Our findings support a growing body of research exploring the impact of trees on speleothem paleoclimate proxies.

1. Introduction

Karst architecture determines the flow and storage of water from the surface to the underlying cave and is a major influence on drip discharge. Karst systems are characterised by three principle flow types. Primary flow occurs where the water travels through the primary porosity of the rock matrix, secondary flow pathways are characterised by water transported along fractures in the bedrock and tertiary flow pathways consist of conduits enlarged by dissolution. The dominance of a particular flow regime changes over time, for example, older limestone tends to have higher secondary porosity (more fractures and enlarged conduits) and a lower primary porosity due to compaction or cementation (Ford and Williams, 1994). The relationship between karst architecture and delivery of water to cave drip discharge sites has been studied to constrain uncertainty in paleoclimate studies (Bradley et al., 2010; Markowska et al., 2015), identify suitable speleothems as climate archives (McDonald and Drysdale, 2007) and in conjunction with drip water geochemistry to determine water residence times in karst aquifers (Arbel et al., 2010; Fairchild et al., 2000; Lange et al., 2010; Sheffer et al., 2011; Tooth and Fairchild, 2003; Treble et al., 2013b). Recent research examining drip hydrology and fluctuations in drip rate have used

hydrological response to characterise flow paths. For example, Markowska et al., (2015) used statistical analysis of drip hydrology data to identify storage flow, in both the epikarst and overlying soil, to develop conceptual models of a karst system.

Over a timescale of months to years, fluctuations in drip discharge are typically driven by seasonal variation in water availability (Hu et al., 2008; Sondag et al., 2003) and long-term climate forcings such as the North Atlantic Oscillation or El Niño-Southern Oscillation (McDonald, 2004; Proctor et al., 2000). On a daily to weekly timescale, drip rate responds to individual rainfall events (Baldini et al., 2012) and barometric changes (Genty and Deflandre, 1998; Jex et al., 2012; Tremaine and Froelich, 2013). Tremaine and Froelich (2013) found weekly and daily fluctuations at one drip site where an increase in barometric pressure decreased volumetric drip rate. This was attributed to atmospheric tides, the heating and cooling of the atmosphere, as the diurnal cycles occurred at two hours before the solar noon (S1) and solar midnight (S2) each day. The cave was situated in poorly to moderately indurated Oligocene limestone with a high likelihood of primary porosity (Scott, 2001). Jex et al. (2012) observed a negative correlation between weekly barometric pressure changes and drip rate at two out of forty drip sites monitored at the base of a paleokarst feature in the marmorised and fractured Devonian limestone at Cathedral Cave, NSW. One drip discharge site had a relatively strong anti-correlation (R=-0.52) after accounting for a 40 hr time lag. This relationship was attributed to a two-phase flow, where pressure fluctuations expanded and compressed air bubbles in the water held within the paleokarst in the unsaturated zone.

Non-linear and chaotic behaviour of drip discharge has been observed over very short (second to minutes) timescales. Chaotic drip regimes were first noted by Genty and Deflandre (1998) in the Devonian limestone of southern Belgium (Genty and Deflandre, 1998). Chaotic and non-linear drip responses were also observed at an event-scale in the fractured-rock limestone of Cathedral Cave, NSW (Mariethoz et al., 2012). These were attributed to the filling and draining of subsurface karst stores within a recharge event, with increasing homogenisation of flow with the filling of the stores. Baker and Brunsdon (2003) observed non-linear responses to rainfall in multi-year drip time series from a fractured rock (Carboniferous limestone) in Yorkshire, UK. With the exception of Tremaine and Froeclich (2013), daily fluctuations have not been observed in cave drip water hydrology. In this paper we aim to increase our understanding of karst architecture by using a novel approach, the synchosqueeze transform, to analyse drip discharge time series from 12 drip discharge sites in Glory Hole Cave, SE Australia. This analysis allows us to characterise daily and sub-daily fluctuations in drip rate and identify the processes driving these oscillations. This study has important implications for understanding karst unsaturated flow processes and karstic groundwater recharge. Currently, most karst models use very simplistic representations of unsaturated flow, if it is considered at all (Hartmann et al., 2014a). This study highlights the importance of vegetation dynamics on vadose flow and recharge making it significant to

karst modelling research and speleothem-based paleoclimate studies which focus on the impact of vegetation dynamics on proxy records (Treble et al., 2015, 2016)

2. Field site and methods

2.1 Glory Hole Cave at Yarrangobilly Caves National Park

Glory Hole Cave is part of the Yarrangobilly Caves National Park located in the Snowy Mountains, New South Wales, Australia (35°43'29.3"S 148°29'14.9"E) at an elevation of 980 m (Australian Height Datum). The Snowy Mountains forms part of the Great Dividing Range, a mountainous region stretching along the eastern seaboard from Queensland to Victoria. The region is sub-alpine and the climate is classified as temperate montane with mild summers and no dry season (Köppen climate classification Cfb) (Peel et al., 2007; Stern et al., 2012).

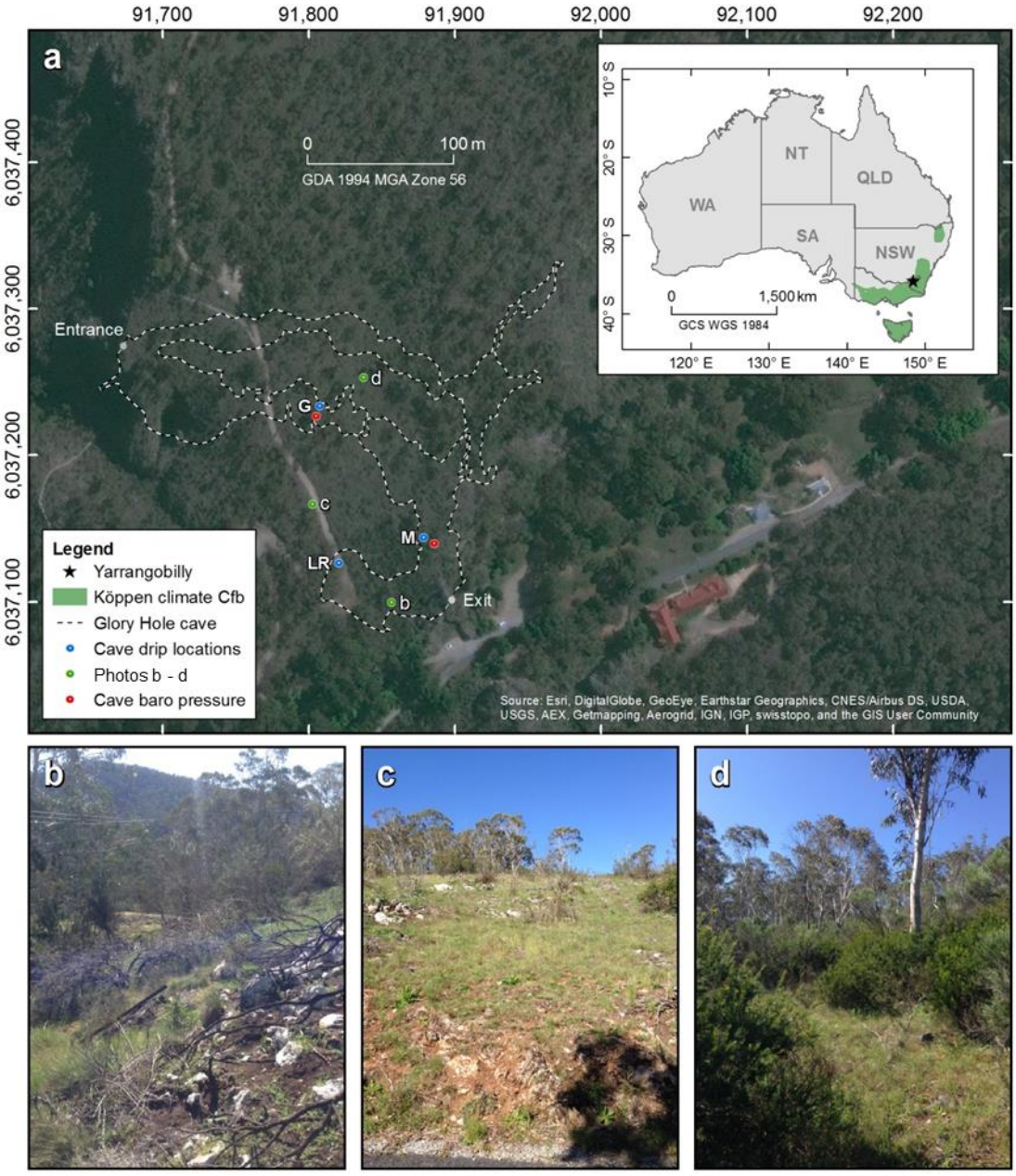

Figure 1 location of Yarrangobilly Caves in New South Wales, Australia with photos of surface vegetation b-d. Extent of Köppen climate zone is from Peel et al. (2007).

Glory Hole Cave is formed of two main sections connected by a narrow constriction ~2 m x 6 m. It is ~243 m in length and is ~100 m at its widest point. The cave extends more than 40 m below the surface in an unsaturated zone of westward sloping limestone bedrock with a contributing catchment area of ~1 km^2. The cave is situated within a formation of massive limestone approximately 12 km long and on average 1 km wide (Worboys, 1982). The limestone is typical of south-eastern Australian limestone; it is Silurian, highly fractured and marblised with little primary porosity. The bedding planes of the limestone are generally obvious with a westward dip (Adamson and Loudon, 1966). It is likely that Glory Hole Cave was formed by water running off less permeable rocks to the east of the limestone, sinking to the water table and rising through large springs close to the Yarrangobilly River (Spate, 2002) which is situated in a gorge in <100 m west of the cave entrance. Glory Hole Cave is likely to be relevant for paleoclimate proxies as it is well decorated and in close proximity (<100 m) to caves that have been used in multi-proxy speleothem based paleoclimate studies (Markowska et al., 2015; Webb et al., 2014).

The vegetation is classified as sub-alpine open snowgum (*Eucalyptus pauciflora subsp. pauciflora*) and black sallee (*E. stelullata*) woodland.

2.2 Cave and surface monitoring

Drip discharge rate was recorded at 12 drip sites in three locations (Fig. 1 and Table 1) within Glory Hole Cave using Stalagmate© drip loggers between December 2012 and September 2015, and monitoring is ongoing. The drip sites were chosen using a stratified sampling method. A transect of the cave was used to select three locations (G, M and LR) that satisfied the following criteria 1) there were actively dripping speleothems, 2) spatially distant from the other locations and 3) different depths within the cave. Individual drips were sampled randomly at each location, with selection guided by practical constraints such as stalagmite surface being suitable for placement of logger and the drip falling from high enough to activate pressure sensor on the logger. Drip loggers recorded the frequency of drips falling onto the surface of the sealed box containing an acoustic sensor in 15 min intervals. The number of drips were converted to ml min^{-1}, assuming that 1 drip equals 0.19 ml (Collister and Mattey, 2008; Markowska et al., 2015). Recently, automated drip loggers have been widely used in cave hydrology research (Cuthbert et al., 2014b; Hu et al., 2008; Mahmud et al., 2015; Rutlidge et al., 2014; Treble et al., 2013a) as they provide a more convenient and efficient way of recording higher temporal resolution data than traditional drip counting methods.

Table 1 Summary of drip sites and location within cave as indicated in Fig. 1, the mean and standard deviation (std) of total flow volume and maximum and minimum drip rate in summer (December- February) and winter (June- August).

		Total flow volume (L)				Drip rate (ml min^{-1})			
		Summer		Winter		Summer		Winter	
Site	Location	mean	std	mean	std	Maximum	Minimum	Maximum	Minimum
G1	G	72.67	9.21	209.58	107.78	19.51	1.84	56.75	0.00
G3		23.76	10.13	115.44	8.37	7.00	0.00	34.43	0.00
G6		3.73	1.90	16.45	0.10	1.43	0.10	4.10	0.65
G8		6.36	0.49	5.81	0.16	1.11	0.00	0.96	0.34
G10		32.47	23.08	104.54	73.58	9.97	0.04	27.27	0.00
G12		6.57	5.71	9.74	4.39	1.68	0.00	2.04	0.43
LR1	LR	32.31	23.93	98.62	7.39	58.30	0.00	57.77	0.00
M1	M	0.29	0.18	0.47	0.00	0.13	0.00	0.11	0.00
M2		7.67	12.85	120.09	21.21	42.53	0.00	74.30	0.00
M4		0.88	1.47	33.95	5.17	4.02	0.00	28.45	0.00
M10		24.53	34.68	127.79	51.36	13.95	0.00	27.56	0.00
M13		7.33	5.05	67.03	6.60	12.40	0.09	41.80	0.92

Barometric pressure and air temperature were recorded at two locations within the cave (Fig. 1) using Solinst level loggers at 15 min intervals from January-September 2015. Precipitation (accuracy ± 4% of total mm), wind speed (accuracy ± 0.1 kph), relative humidity (accuracy ±2%), air temperature (accuracy ± 0.5 °C) and barometric pressure (accuracy: ±1.0 kPa) were measured with a Davis Vantage Pro 2 weather station <1 km from Glory Hole Cave at 15 min intervals and data stored using a Datataker DT80 data logger. Solar radiation (MJ m^{-1}) was derived from satellite imagery processed by the Bureau of Meteorology from the Geostationary Meteorological Satellite and MTSAT series.

Daily potential evapotranspiration was estimated using ETo Calculator software developed by the Land and Water Division of the Food and Agriculture Organisation of the United Nations http://www.fao.org/nr/water/eto.html. The software is based on the Penman-Monteith equation and is a physically-based method with physiological and aerodynamic parameters. The climate parameters used were air temperature (mean, maximum and minimum), relative humidity (mean, maximum and minimum), wind speed and solar radiation.

2.3 Spectral analysis of cave drip discharge rates

A new advance in signal processing was used to analyse the frequency-time content of measured cave drip discharge rate, temperature and barometric pressure. Daubechies et al (2011) first presented the synchrosqueeze transform (SST) as an empirical mode

decomposition like tool for disentangling a complex signal into approximately harmonic componentsThakur et al (2013) adapted the SST to discretised data (rather than continuous functions) and developed a MATLAB Synchrosqueeze Toolbox (available for download: https://web.math.princeton.edu/~ebrevdo/synsq/) which efficiently implements the SST algorithm and offers a log2 frequency resolution. They further tested the robustness properties of SST and found that it precisely estimated key signal components, and that it was stable against errors and noise (Thakur et al., 2013). The SST combines advantages of the wavelet transform in regards to frequency resolution with the frequency reallocation method (Auger and Flandrin, 1995) in order to reduce spectral smearing when mapping out the frequency-time content of a complex signal. This presents a significant advantage when identifying multiple frequency components over traditional methods such as the Fourier, or more recently the Wavelet transform.

Identification of continuous time periods featuring multiple distinct frequency components that are buried in a signal

Methodology steps	**Comment**
1. Measure parameter	For example drip discharge rate [M^3/T], temperature [°C], barometric pressure [kPa]
2. Use the MATLAB Synchrosqueeze Toolbox (Thakur et al., 2013) to calculate the frequency domain response $\mathcal{F}_{f,t}$ f is frequency (in log_2 resolution) [1/T] • t is discrete time (sampling resolution) [T]	The output is a 2D matrix containing the complex frequency domain response with elements corresponding to discrete frequency values (as rows) and time values (as columns)
3. Calculate signal amplitudes $A_{f,t} = \lvert\mathcal{F}_{f,t}\rvert = \sqrt{\Im(\mathcal{F}_{f,t})^2 + \Re(\mathcal{F}_{f,t})^2}$	Standard procedure to calculate the amplitude of a signal component (length of complex frequency domain vector)
4. Normalise signal amplitudes $a_{f,t} = \frac{A_{f_{min}<f<f_{max},t}}{max(A_{f_{min}<f<f_{max},t})}$ $f_{min} = 0.48$ and $f_{max} = 4.1$	The base for this normalisation allows focus on a desired frequency range. This is especially useful to identify continuous periods of weaker frequency components in the presence of other, stronger components or chaos
5. Visualise normalised amplitudes in pseudo-colour plot	Colour scale can be customised
6. Identify continuous time periods with multiple distinct frequency components based on the visual observation of continuous relative amplitudes in the desired frequency axis	While this step is conducted manually, it could be automated using criteria for the strength and continuity of any stable frequency component amplitudes of interest

Figure 2 Overview of the methodology applied to identify continuous time periods of multiple distinct frequency components buried in a measured time series.

The drip discharge rate time series, barometric pressure and air temperature (potential weather related drivers of drip discharge oscillations) were directly used as an input for the MATLAB SST Toolbox. The calculated output is a complex frequency domain response, as is

common for signal component decomposition, but in matrix form $\mathcal{F}_{f,t}$ mapped over frequency (rows) and time (columns). Amplitudes were calculated as the length of the complex frequency response vector $A_{f,t} = |\mathcal{F}_{f,t}|$ and then normalised to obtain relative amplitudes $a_{t,f}$, using the maximum amplitude value occurring within the desired frequency range $0.48 < f < 4.1$ and within the timespan of interest (e.g., plot). The relative amplitude of all parameters was visualised using pseudo-colour plots showing the spectral content of the signal. These plots allowed visual identification of key frequency components that could easily be distinguished from chaos, i.e. lack of regular oscillations identified as signals with varying amplitude and frequency over time. Stronger periodic components would yield a larger amplitude on the respective frequency scale and therefore also a colour that was closer to 1 in each of the SST plots (refer to the individual colour legends for values).

A periodic drip discharge rate could be defined as consisting of continuous periods of a) stable 1 cycle per day (cpd) frequency, b) stable 1 cpd and 2 cpd frequency, c) chaos (components with randomly varying frequency and amplitude). We used a) and b) as spectral "fingerprints" to identify and mark periods of continuous occurrence of daily and sub-daily oscillations in the drip discharge rate dataset. While identification of periodic signal components through visual inspection was subjective, it is based on a set of objective indicators such as normalised amplitude values and defined criteria. This methodology is summarised as a sketch in Figure 2 and could be applied to any type of time series in order to map the signal frequency content and identify periods with multiple distinct frequencies of interest.

3. Results

3.1 Drip discharge rate time series

The drip discharge time series are presented in Fig. 3. The drip discharge sites are spatially clustered in three groups within the cave (Fig. 1 and Table 1). Sites with the G prefix are located near the main entrance of the cave on the western side. The location is highly decorated with speleothems. M sites are located in the middle section of the cave in a large chamber with a high ceiling populated by soda straw formations. Location LR1 is situated near the cave exit at the top of a flow stone.

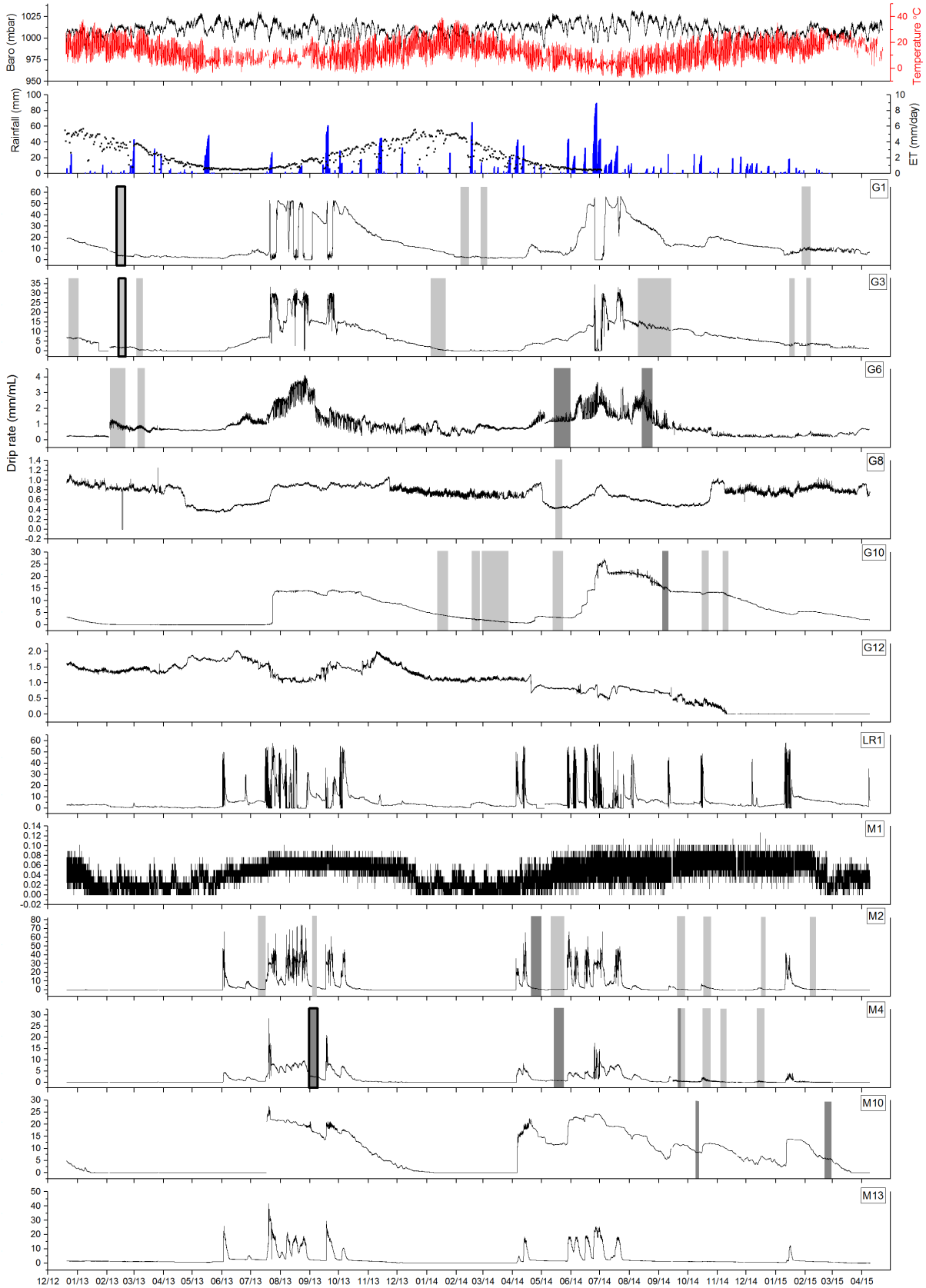
Baro (mbar)
Temperature °C
Rainfall (mm)
ET (mm/day)
Drip rate (mm/mL)
G1
G3
G6
G8
G10
G12
LR1
M1
M2
M4
M10
M13
12/12 01/13 02/13 03/13 04/13 05/13 06/13 07/13 08/13 09/13 10/13 11/13 12/13 01/14 02/14 03/14 04/14 05/14 06/14 07/14 08/14 09/14 10/14 11/14 12/14 01/15 02/15 03/15 04/15

216

217

Figure 3 Drip discharge rate time series for all drip sites in Glory Hole Cave with periods where daily fluctuations occur highlighted in light grey (1 cpd) and dark grey (1 cpd and 2 cpd). The time periods examined in more detail in Fig. 4, 5 and 6 are indicated by bolder outline. Daily evapotranspiration (19/12/2012- 03/07/2014), rainfall, barometric, air temperature and are also shown.

The drip discharge rate at G1 and G3 varies seasonally, with higher drip rates in winter, total flow volume of 133.37 L and 109.52 L, respectively, than summer (64.56 L and 14.1 L, respectively). Drip rate increases in response to rainfall events during the wet season and gradually decreases through the drier part of the year. Drip rate is lowest during April and May and highest during June and July. Similarly, G6 exhibits seasonal variation with a higher volume of discharge during the winter than summer. The drip rate at G10 increases sharply from 0.14 ml min^{-1} on 21/07/2013 to 13.75 ml min^{-1} on 29/07/2013, this drip rate is consistently sustained for 3 months indicated by the flat topped hydrograph (Fig. 3). From July 2013 onwards, the drip rate gradually decreases until June 2014 where it increases sharply again by an order of magnitude from 2.03 ml min^{-1} on 3/06/2014 to 24.96 ml min^{-1} on 4/07/2014. In May 2014, the drip rate again rapidly increases at G10 from 0.142 ml min^{-1} to 21.59 ml min^{-1} on 18/04/2014 and then proceeds to gradually decline until April 2015 where it reaches baseline conditions. M10 exhibits similar behaviour with a low baseline drip rate which increases sharply during July 2013 and is sustained for ~3 months, however, the elevated drip rate decreases more rapidly than G10, returning to baseline conditions in January 2014. M1 has a very low drip rate ranging from 0- 0.13 ml min^{-1} and is seasonally variable with higher drip rates during the winter. LR1, M2, M4 and M13 are very responsive to infiltration events and are characterised by a 'flashy' flow type, evidenced by the frequent spikes in drip rate. G12 has a low discharge rate which gradually decreases over the monitoring period until the site dries up completely in November 2014. There are small variations in drip rate that are not associated with rainfall events or seasonal drying. G8 is the only site which has a lower total flow volume during the winter (2013= 5.92 L; 2014= 5.7 L) than summer (2014= 6.39 L; 2015= 6.84 L).

3.2 Characterisation of oscillations in the drip discharge rate

Daily fluctuations in drip discharge rate were identified in eight out of twelve sites using SST. There was no connection between the sites that did not exhibit the fluctuations with respect to spatial location, flow volume or flow regime type. The temporal and spatial pattern of daily oscillations are shown by the grey shaded areas in Fig. 3. The length of time the signal is present varied temporally for each drip site. For example, there was a strong 1 cpd signal in the drip water at G1 for 10 days in February 2013 whereas in January 2014 1 cpd fluctuations only lasted 5 days (Fig. 4). The timing of when the signal occurs on an annual scale varied within and between drip sites. For example, a 1 cpd signal only occurred during the first 3 months of the year for G1, whereas a 1 cpd signal occurred sporadically at

G3 throughout the calendar year (December 2012, February and March 2013, January 2014, September 2014, January 2015).

The daily timing of minimum and maximum drip rate varied within and between individual drip sites. At G1 the 1 cpd minimum and maximum drip rate generally appeared between 12- 9 am and 3pm-12am, respectively. Daily oscillations were only observed once at G8 between 14-21/05/2014 with minimum drip rate appearing 9pm and maximum drip rate appearing around 12 pm. Both 1 cpd and 2 cpd signals were observed at M10 for all the periods of drip rate oscillation with the larger peak occurring in the afternoon between 12-6 pm and the smaller peak between 12-6 am, minimum drip rate appeared consistently between 6-9 am. Time lag between drip rate and air temperature was quantified by performing a cross correlation analysis with a shift interval of 15 mins up to $\pm$24 hours (Table 2). The lag time was identified as the point of maximum negative correlation between the two variables with the exclusion of sites with missing data. At most sites the lag time between maximum air temperature and minimum drip rate varied greatly over the monitoring period. For example, at M4 initially the lag time was 24 hours in September 2013, decreasing to 9 hours in May 2014 and eventually levelling off at around 16 hours from September to December 2014. In contrast, G1 had a similar lag time over all 4 periods of drip rate fluctuation ranging from 11.25- 12.75 hours. G6 was unique in that the minimum drip rate occurred before the maximum air temperature in February and March 2013, January 2014 and 2015. Analysis of variance indicated that drip site and season did not explain a significant amount of variance in lag time.

Table 2 shows the time lag calculated using cross correlation analysis between air temperature and daily drip rate for each period of drip rate oscillation.

	Drip rate oscillation			
Site	**Start**	**End**	Time lag (hours)	R^2
	11/02/2013	21/02/2013	-11.5	-0.82
	4/02/2014	14/02/2014	-12.75	-0.55
	27/02/2014	10/03/2014	-11.25	-0.37
G1	27/01/2015	5/02/2015	-11.5	-0.69
	23/12/2012	2/01/2013	-23.25	-0.46
	12/02/2013	20/02/2013	+2	-0.56
	4/03/2013	10/03/2013	+1	-0.44
	6/01/2014	20/01/2014	+7	-0.62
	20/09/2014	29/09/2014	-4	-0.38
	16/01/2015	20/01/2015	+0.25	-0.59
G3	3/02/2015	6/02/2015	+1	-0.74
	3/02/2013	19/02/2013	-4	-0.19
G6	5/03/2013	12/03/2013	-3.25	-0.51

	13/05/2014	29/05/2014	-21	-0.50
	14/08/2014	24/08/2014	-7	-0.50
G8	14/05/2014	21/05/2014	-9.5	-0.55
	5/10/2013	16/10/2013	-24	-0.40
	5/01/2014	22/01/2014	-0.5	-0.32
	18/02/2014	24/02/2014	-3	-0.46
	4/03/2014	23/03/2014	-2.75	-0.47
	13/05/2014	23/05/2014	-15	-0.37
	16/10/2014	22/10/2014	-23	-0.49
	8/11/2014	12/11/2014	-1.5	-0.59
G10	5/02/2015	25/02/2015	-0.25	-0.33
	3/09/2013	7/09/2013	-15.25	-0.76
	20/04/2014	28/04/2014	-1	-0.40
	13/05/2014	21/05/2014	-17.75	-0.60
	20/09/2014	28/09/2014	-23.75	-0.40
	18/10/2014	25/10/2014	-2	-0.31
M2	5/02/2015	10/02/2015	-20.75	-0.51
	2/09/2013	8/09/2013	-24	-0.46
	14/05/2014	23/05/2014	-9	-0.38
	21/09/2014	28/09/2014	-16.25	-0.59
	16/10/2014	24/10/2014	-16.25	-0.65
	4/11/2014	13/11/2014	-16.5	-0.62
M4	12/12/2014	22/12/2014	-16.5	-0.32
	23/12/2012	26/12/2012	-24	-0.32
M10	9/10/2014	12/10/2014	-4.75	-0.46

1 cpd and 2 cpd signals can occur concurrently, for example, at M4 between 1-9/9/2013 (Fig. 5). This trend, where the 2 cpd is weaker than the 1 cpd is consistent across all sites where the two signals coincide. The 2 cpd signal can be visually determined in the raw drip rate data by a second smaller peak (Fig. 5). Examples of characteristic SST plots alongside the corresponding raw drip rate and surface temperature data will be discussed in greater detail below. All SST analyses have been plotted in the SI.

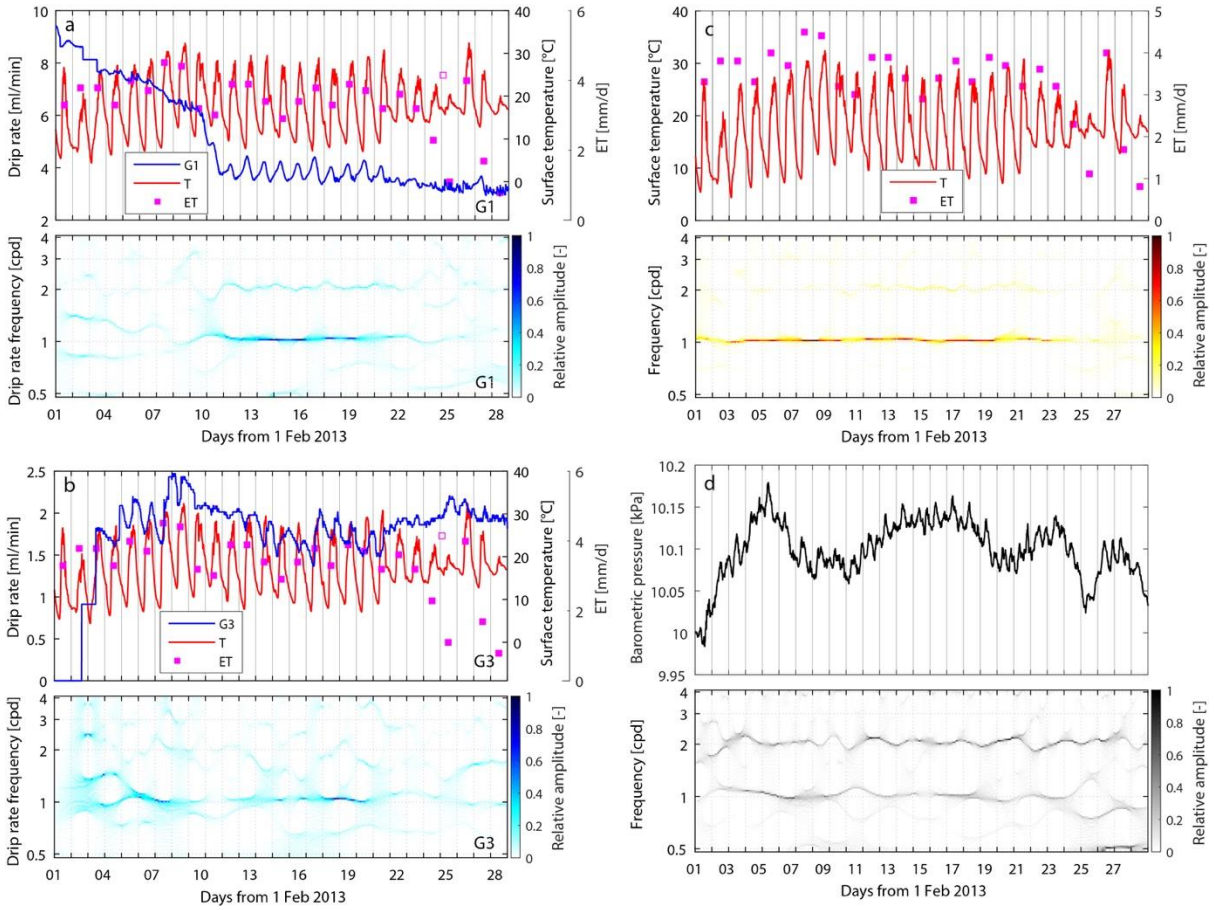

290

291 Figure 4 shows the raw drip rate, evapotranspiration and surface temperature data with the
292 corresponding drip rate synchrosqueezing plot for time periods where a 1 cpd signal is
293 present for sites a) G1 and b) G3 c) surface air temperature (T) and potential
294 evapotranspiration (ET) and d) barometric pressure for period February 2013.

295

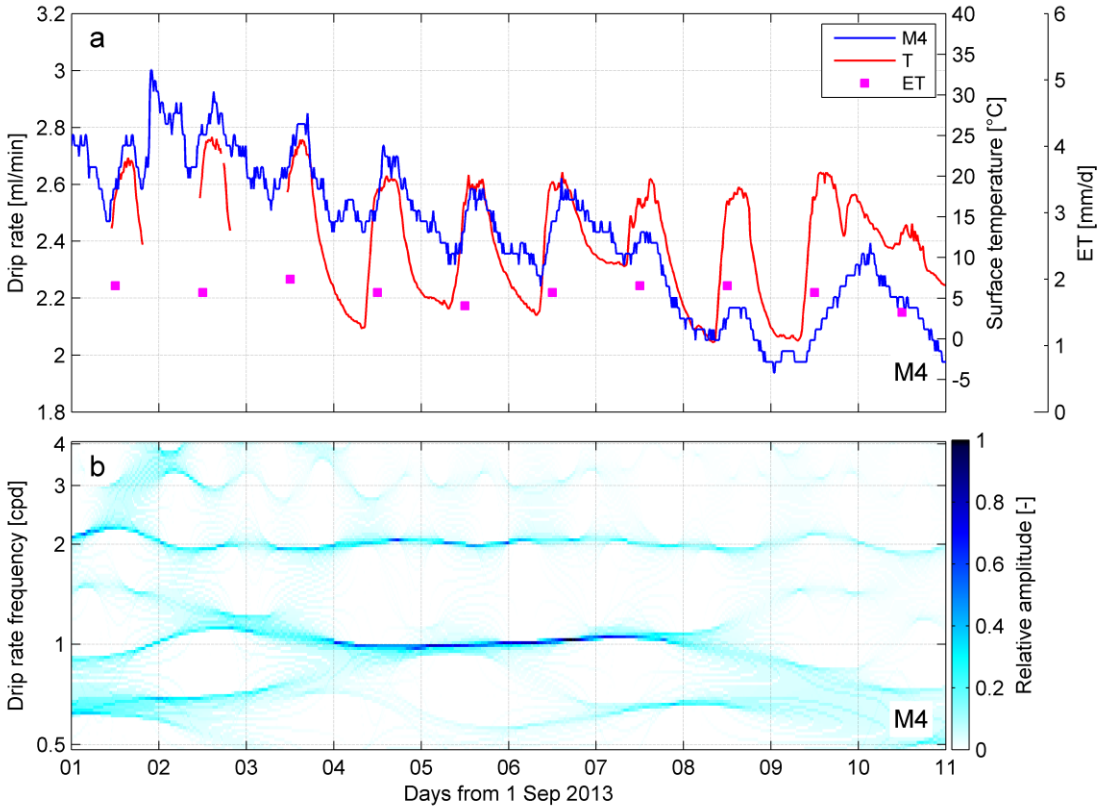

Figure 5 shows the raw drip discharge data, evapotranspiration, surface temperature and synchrosqueeze transform (SST) plot of the drip discharge for site M4 from 1-11/09/2013.

SST identified a 1 cpd oscillation in drip rate between 08/02/2013 and 21/02/2013 at G1 and G3 (Fig. 4a, b). At G1 (Fig. 4a), the signal was initially chaotic, but from 08/02/13- 21/02/13 the drip rate oscillates sharply at 1 cpd. The maximum drip rate ranging from 4.03-3.75 ml min-^{1} occurred between 9:18 and 10:27 and the minimum drip rate ranging from 3.34 -3.75 ml min^{-1} occurred between 18:39 and 21:27. The signal was chaotic from 21/02/2013.

The drip rate at G3 (Fig. 4b) oscillated at 1cpd for 8 days from 12/02/13-20/02/13. In contrast to G1, the maximum drip rate appeared in the evening and the minimum drip rate occurred in the morning. The maximum drip rate ranging from 1.63 -2.01 ml min^{-1} occurred between 20:21 and 00:40 and the minimum drip rate ranging from 0.36-0.48 ml min^{-1} occurred between 9:03 and 11:36 with the exception of 15/02/13 and 18/02/13 where it appeared at 14:06 and 12:57, respectively. Similar to G1, the 1 cpd trend descended into chaos from 20/02/13 onwards. The maximum drip rate occurs between 14:23 and 22:45 and ranged from 0.53 to 1.14 ml min^{-1}. The minimum drip rate occurred between 01:18 and 11:32 and ranged from 0.228 to 0.95 ml min^{-1}.

From 01-27/02/13, daily barometric pressure peaked between 8:30-9:00 with a magnitude of 0.1-0.5 kPa with a smaller second peak between 20:00-22:00 with a magnitude of 0.1-0.3 kPa (Fig. 4c). There were larger changes in air pressure on a mesoscale with peaks in air pressure on 16/02/13, 22/02/13, 26/02/13 and minimum air pressure on 19/02/13, 24/02/13 and 28/02/13. The air pressure changes in these cycles were as much as 1.5-2 kPa. The drip rate at G1 and G3 did not appear to be affected by the daily or weekly changes in air pressure. For example, when air pressure decreased dramatically on 27/02/13 (Fig. 4c) there was no substantial change in drip rate at either G1 or G3.

Insolation drives daily cycles in surface air temperature with maximum temperatures recorded between 11:30-16:00 and minimum temperatures recorded between 4:00-8:00 (Fig. 4d). The difference in daily minimum and maximum air temperature varied greatly. For example, between 12- 20/02/2013 the difference was 17.05-22.2 °C whereas between 21-27/02/2013, the temperature difference was as little as 4.5 °C. Evapotranspiration ranged from 0.8- 4.5 mm/day and was relatively high from 1-23/02/2013 with a slight downward trend which then decreased sharply on 23/02/2013 and 24/02/2013 to 2.3 mm/day and 1.1 mm/day, respectively. Evapotranspiration had a strong correlation with maximum daily air temperature (R^2= 0.59, p-value <0.05).

4. Discussion

4.1 Cave drip rate and karst architecture

The complexity of the Glory Hole Cave karst system is evident in the variety of drip regimes. For example, the drip rate at G1, G6 and G3 is seasonally driven with high discharge rates during the wettest period of the year. In contrast, drip discharge at G10 and M10 is likely driven by a storage component which discharges via a less permeable pathway which limits the store at a particular level during wet periods. The drip site is fed via the main water store rather than the overflow pathway itself (Baker et al., 2012; Bradley et al., 2010). Sites LR1, M4, M13 and M2 behave similarly in that they are all very responsive to rainfall events and have low base flows during periods of low rainfall. The response to rainfall events occur within 24 hours across these sites. Calculated flow volumes indicate the storage capacity of the stores feeding the discharge sites. For example, there was an infiltration event on 01/06/2013 which caused a dramatic increase in drip rate for sites LR1, M2, M4 and M13. The flow volumes for each site from the start of the event to the point where the discharge returns to a constant rate are as follows LR1 (1.60 L), M4 (2.99 L), M13 (8.09 L) and M2 (11.30 L). The length of the recession limb, calculated from the peak of the hydrograph until the drip rate returns to base rate, is indicative of the speed at which the store drains. For example, the decay in drip rate is 12 days for site M2 compared to 4 days for M13. The time it takes for the store to drain is not dependent on flow volume, as M13 has a flow volume of more than 5 times that of site LR1 but they both have drainage periods of 5 days. The discrepancy in drainage time could indicate variation in flow pathway length between sites. G8 is the only site with a relatively lower total flow volume during winter than summer. M1 has a low drip rate that shows a small seasonal fluctuation but does not visibly respond to individual events. This site is likely being fed by a store that is large enough to assimilate short term inputs from the surface without impacting drip rate. This type of store has been described as a karst hydrological model component in a number of studies (Arbel et al., 2010; Hartmann et al., 2014b; Markowska et al., 2015).

4.2 Daily oscillations in drip rate

Constant frequency oscillations in drip discharge (1 cpd and 2 cpd) occur sporadically throughout the monitoring period December 2012- April 2015 at 8 out of 12 monitored drip sites. This phenomenon could be explained by a number of daily drivers including variations in pressure gradients between karst and cave due to cave ventilation effects, atmospheric and earth tides, or variations in hydraulic conductivity (due to changes in viscosity of water with daily temperature oscillations), and solar driven daily cycles of vegetative (phreatophytic) transpiration. These drivers are now considered in turn.

4.2.1. Cave ventilation effects

Surface air pressure and cave air pressure were significantly correlated (τ= 0.82 significant at 95%, n=8939) for the monitoring period 19/01/2015-08/09/2015. This indicates that cave air exchange ("breathing" or ventilation) is very efficient and consequently that variations in air pressure between the cave and surface can be ruled out as driving the fluctuations in drip rate.

4.2.2. Barometric loading

Atmospheric tides are caused by changes in air pressure due to the heating and cooling of air masses during the day and night. Correlations between atmospheric tides and drip rates can occur since increases (decreases) in atmospheric pressure at the ground surface are partitioned into stress increase (decrease) in the soil/rock mass and pore pressure increase (decrease) within the formation (Acworth et al., 2015). Drip rates could be affected if this changes the pressure gradient between the groundwater in karst stores and the cave (Tremaine and Froelich, 2013). Such a pressure imbalance is dependent on the hydromechanical properties and karst architecture as well as the degree of pneumatic connection between both the surface and the water table, and the surface and the cave at the location of the drip. Maximum and minimum atmospheric pressure occur at the same time each day (Fig. 4d).

Atmospheric tides were eliminated as a process to explain the daily oscillation phenomenon for several reasons. Firstly, there was no relationship between drip discharge rate and the longer term barometric changes caused by synoptic weather patterns (Fig. 4). The mesoscale fluctuations in pressure caused by synoptic weather patterns are an order of magnitude higher than those caused by daily atmospheric tides. Since the drip rate did not respond to pressure changes of this size, they will not respond significantly to changes of a smaller magnitude at a higher frequency because higher frequency signals will be more highly damped and lagged. Secondly, the timing of the daily maximum and minimum drip rates in Glory Hole Cave varied within each drip site over time. For example, the peak discharge time for site G6 varied between 13:24 and 19:48 for the period 11/08/2013-25/08/2015. This finding contrasts with previous studies where drip rate is negatively correlated with barometric pressure and responds to daily pressure changes linearly (Tremaine and Froelich, 2013). However, this could indicate that the daily drip water variations in Glory Hole Cave are being driven by a non-linear process and this is discussed further below. Thirdly, the karst architecture of Glory Hole Cave is well-developed, has little to no primary porosity and is unconfined. Hence, it is unlikely to exhibit barometric responses such as seen in confined systems (Merritt, 2004), whereby pore pressure changes due to barometric loading are substantially lower than the change of cave air pressure.

4.2.3. Earth tides

Earth tides are solid deformations of the Earth's surface caused by the gravitational pull of the moon and sun (Merritt, 2004). It has been previously shown that earth tides can cause regular oscillations in groundwater level if the aquifer is sufficiently confined (Acworth et al., 2015). However, at Glory Hole Cave this process can be ruled out due to the unconfined conditions, the fact that the compressibility of limestone is smaller than that of water, and because fluctuations in pressure caused by earth tides are so small.

4.2.4. Temperature driven viscosity influences on hydraulic conductivity

The study site has large surface temperature variations, particularly in summer where day time and night time temperatures can vary up to 31.1 °C. Consequently, the dynamic viscosity of water could range from 0.8- 1.79 x 10^{-3} Pa s (based on a temperature range from 30-0 °C, respectively). However, the conductive propagation in diel temperature variations are expected to be highly attenuated with depth (Rau et al., 2015) resulting in almost complete damping by 1 m bgl. Furthermore, the daily temperature range within the cave itself is just 0.08-1.53 °C, primarily due to air exchange moderated by conductive equilibrium with the cave walls. The variation of water viscosity (which is inversely proportional to hydraulic conductivity) is approximately 2 to 3 % per degree in the range 10 to 30 °C. Considering that the amplitude of a 1 cpd drip rate fluctuation can be as much as 75 % of the maximum drip rate, the greatest anticipated change in hydraulic conductivity, and therefore the drip rate (proportional to the hydraulic conductivity by Darcy's law), on a daily cycle, is likely to be 2-3 orders of magnitude lower than the observed variation in drip rate on a daily basis. We therefore conclude that the daily fluctuations in drip rate are unlikely to be caused by variations in hydraulic conductivity due to changes in viscosity of water.

4.2.5. Solar driven daily cycles of vegetative (phreatophytic) evapotranspiration

The timing of the daily drip rate signal appears to be associated with the difference in maximum and minimum surface temperature. In the examples examined in more depth in Fig. 4a-b, when the difference between the maximum and minimum temperature was high (17- 22 °C) and the evapotranspiration was relatively high (mean 3.6 mm/day) the 1cpd signal was continuous. Conversely, when the temperature difference was small (4.5-12.7 °C) and the potential evapotranspiration was relatively lower (mean 2.2 mm/day), the 1 cpd signal dissolved into chaos.

During periods when there are 1 cpd oscillations in drip rate, there was a relationship between drip rate and surface temperature on a weekly timescale. The best example, in Fig.

6 where τ= -0.21 (significant at 95%) for a 2-day average air temperature and drip rate at G1 from 01-19/02/2014.. We have demonstrated above that it cannot be air temperature driving the signal through either atmospheric tides or water viscosity changes. However, the relationship between surface temperature variability and 1 cpd drip rate oscillations could be explained if the association with diurnal temperature variability is due to variations in solar radiation received at the surface, as it is solar radiation which primarily drives photosynthesis and thus transpiration in vegetation. This is confirmed by the strong positive relationship between daily solar radiation and potential evapotranspiration (R^2= 0.59, p-value <0.05).

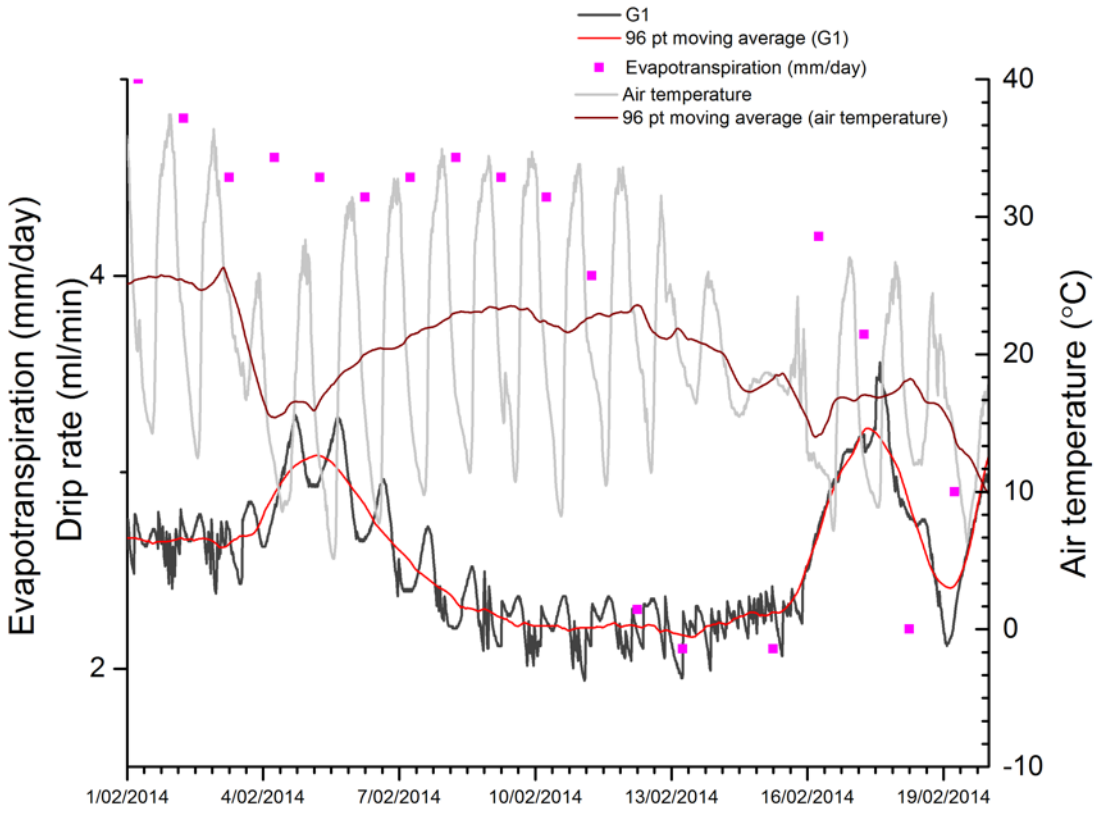

Figure 6 shows the surface air temperature, evapotranspiration and drip discharge rate with the corresponding daily moving average for site G1 01/02/2014-19/02/2014.

Daytime solar radiation receipt is highest in the absence of cloud cover, because there is no barrier to incoming short wave radiation which leads to the heating of the earth's surface and atmosphere, resulting in higher air temperature. Due to the lack of cloud cover, night-time cooling occurs because of the heat loss through outgoing long wave radiation, therefore periods of high daytime solar radiation are characterised by large air temperature amplitudes. In comparison, solar radiation received at the earth's surface is low in the

presence of cloud cover because of the high albedo of clouds. In this case, there is a smaller temperature amplitude because clouds reduce the amount of incoming short wave radiation during the day, reducing daytime temperatures and reduce the amount of outgoing longwave radiation and effectively "insulating" the air at night leading to relatively warmer temperatures at night. During periods of high solar radiation, plants photosynthesise more and therefore use more water. We hypothesise that firstly, tree water use was driving the intermittent daily oscillations in drip discharge demonstrated by the relationship between daily to weekly variations in surface air temperature and drip discharge and secondly, the sporadic nature of the oscillations was driven by complexities in the karst architecture. It has been widely accepted that tree water use causes fluctuations of the water table (Gribovszki et al 2010; Acworth et al 2015). However, this is the first study that shows tree water use affecting cave drip water.

The area above the cave and in the small uphill catchment is dominated by *E. pauciflora* and *E. stelullata* (Fig. 1). Eucalypt species have a bimodal root system with shallow lateral roots and vertically descending roots which penetrate into the profile to depths of up to 18 m, with depth depending on soil characteristics and the degree to which the bedrock is fractured and conduits developed (Crombie, 1992; Farrington et al., 1996). Hence, these trees have the mechanism to abstract water from karst stores at depth which supports our theory that tree water use causes daily oscillations in cave drip rate.

Tree water use from deep roots occurs when the upper layers are too dry and have a lower water potential than the soil water at deeper levels (Dawson and Pate, 1996; Zapater et al., 2011). Maximum tree water use by the roots is therefore expected in the afternoon during the period of maximum solar radiation, possibly lagged due to the time taken to hydraulically lift the water. Conversely, minimum tree water use is expected at the end of night around 6am. Burgess et al (2001) measured sap flow in Eucalypt tap roots, finding tap root sap flow peaked around 1 pm and negative sap flow values indicated reverse (acropetal) flow between 7pm- 7am. In consideration of this, drip water that comes from fractures and stores which contain tree roots would be expected to have a minimum drip discharge in the afternoon and maximum around sunrise. In reality, we observe more complex daily drip oscillations, with peak drip rate occurring at different times of the day and different times of the year. This is to be expected from a karstified system with flow routed through a varied and complex fractured network. Different scenarios for daily oscillations in a karst system will be discussed in detail below.

4.2.5.1 Scenarios for solar driven daily cycles of phreatophytic evapotranspiration

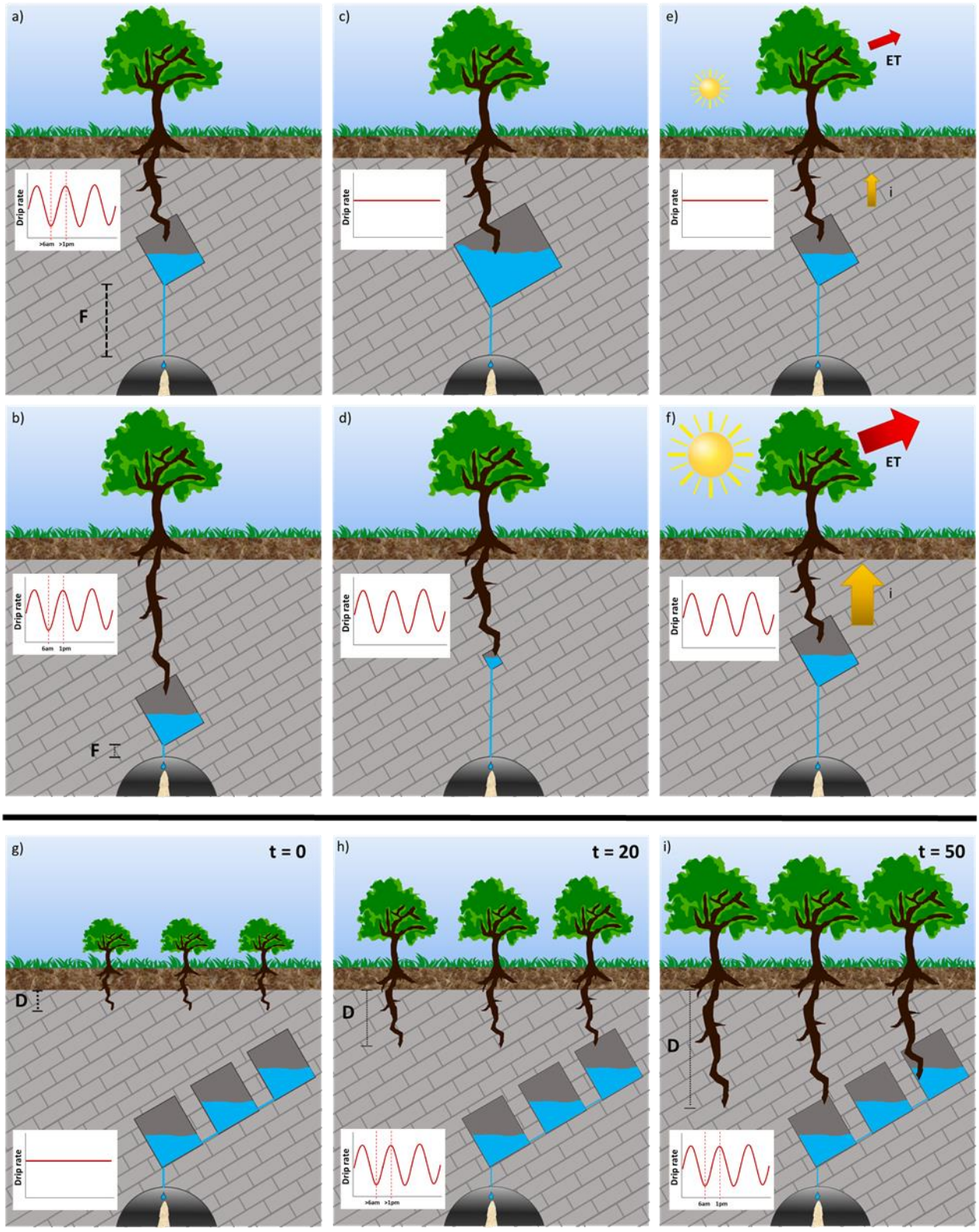

Figure 7 shows a conceptual representation of tree water use from karst stores under different circumstances. a) and b) show different karst store-drip site flow path lengths (F) as the tree roots access karst stores at different depths; c) and d) show tree roots accessing karst stores with different volumes; the influence of annual insolation on evapotranspiration

(ET) and hydraulic lift (i) during winter and summer is shown in e) and f) respectively. Finally, the increase in rooting depth (L) and access to deeper karst stores over time in years (t) is explored in g-i.

The depth of a store could affect the timing of daily drip rate oscillations due to the delay in tree water transport. For example, consider the hypothetical, identical trees with roots intercepting identical karst stores or fractures at *different* depths in Fig. 7a and 7b. There is likely to be a greater lag in drip response in Fig. 7a than Fig. 7b because of the longer flow path-length (F) from the tree root to the cave drip site. Given that eucalypt tap roots can penetrate to depths ranging from 5-20 m with tap root length depending on the depth of accessible water (Carbon et al., 1980; Dawson and Pate, 1996) and the drip sites at Glory Hole Cave are located 30-50 m below the surface, we can speculate that the minimum flow path length between a taproot accessing the karst store and the drip site below could vary from 10-45 m. In reality, it is difficult to calculate exact flow path length because of the prevalence of lateral flow in heavily karstified systems. This has been demonstrated by Markowska et al (2016) in a study where water spiked with a tracer was used to irrigate the surface above a cave resulting in a response at discharge sites located 7 m laterally from the irrigation location. Across all sites, lag time between maximum air temperature and minimum drip rate ranged from 0.25- 24 hours (Table 2). We can hypothesise that those sites with a shorter lag time have a shorter path length from tree root accessed store to cave discharge site than the other drip sites. For example, the lag time for site G1 ranges from 11.25- 12.75 hours whereas site G10 ranges from 0.5- 3 hours. This process could also explain the large variation in lag time within a particular site, for example at G6 the lag time was 21 hours in May 2014 and decreased to 7 hours in August 2014 (Table 2). We hypothesise that the change is due to a shortening of the path length from root accessed store to cave discharge site as the tree grows and increases its rooting depth, thus accessing a deeper water store.

The size of the karst store, or volume of water within the store, could determine whether the daily oscillation is observable or not. Consider the conceptual Fig. 7c and 7d, where identical trees have roots intercepting different karst stores at the *same* depth. We propose that a daily oscillation will only be observed when the tree water use is a significant part of the total water store so a daily oscillation is more likely to be observed in the smaller store (Fig. 7d) than a store with a larger volume (Fig. 7c). The influence of store volume on the presence of daily oscillations could also explain why the phenomenon is not observed at M1. In section 3.1 we discuss how the low, consistent drip rate at M1 responds to seasonal drying but does not respond to individual rainfall events. We propose that this site is fed by a store large enough to assimilate individual rainfall events and the same line of reasoning could explain the lack of response to tree water use, the volume of water extracted by tree roots is insignificant in relation to the large volume of water in the store. Conversely, we can hypothesise that G6 has a small store volume that is more sensitive to water uptake by tree roots, which is why we see the minimum drip rate occurring 0.25-7 hours before peak air

temperature (Table 2). Furthermore, this scenario is supported by the fact that, generally, the daily oscillations are not exhibited during periods of high rainfall, and consequently high drip discharge, as the tree use signal is more likely to be a smaller fraction of the total water volume. Sites G1, G3 M2 and M4 have high seasonal discharge rates during June-September as indicated by the multiple hydrograph peaks for the corresponding sites in Fig. 3. There are no daily oscillations during these periods of peak discharge at any of these sites. Daily oscillations coincide with the receding limb of the peak at sites M4 (July and September 2013) and M4 (September 2013) as the drip rate decreases. The non-observance of daily oscillations during periods of high rainfall could also be attributed to the redistribution of water by the roots from the saturated soil to the unsaturated subsurface (Burgess et al., 2001).

Tree water use responds to annual variation in insolation. Consider Fig. 7e and Fig. 7f where one tree root intercepts the same karst store over the course of a year. During winter (Fig 7e), there is less insolation than the summer (Fig 7f) therefore the rate of evapotranspiration is lower. This means that in winter the hydraulic lift (i) is low or negative and daily oscillations in drip discharge could be dampened or absent. Our analysis reveals that only 2 out of 41 periods of 1 cpd oscillation occur during winter months June-August (G6 between 14-24/8/13 and M2 between 8-13/7/2013). However, our analysis also revealed that season did not explain a significant amount of variance in lag time, thus suggesting that more variables, such as karst architecture, are affecting the timing of drip rate oscillations.

In reality, there are multiple trees of different ages above the cave, further complicating the flow variability. Figure 7g-i presents a conceptual representation of tree tap root length increasing (L) as the tree grows and accesses deeper karst stores over 0-50 yr timescale (t). This response to annual insolation and the interaction of multiple trees of varying ages could explain why daily oscillations at an individual drip site occur one year and not the next, for example at M10 there is a 1 cpd in December 2012 however, this oscillation does not occur at the same time in 2013 or 2014. The mechanism in Fig. 7i could also explain why 2 cpd signals are also observed, whereby multiple tree roots are accessing interconnected water stores at different depths resulting in two separate cycles with differing lag times. The occurrence of 2 cpd signals in drip rate could also be related to signal processing where if the signal is not strictly sinusoidal there may be harmonics in the spectrum. This finding and the interpretation is an area for further research.

4.6 Implications for karst architecture and climate proxy modelling research

Karst architecture controls flow regimes and drip discharge rates of water infiltrating into caves (e.g., Markowska et al., 2015). Flow rate influences speleothem climate proxies, such as the $\delta^{18}O$ and concentration of solutes in drip water, through the dilution and mixing of percolation waters prior to reaching the cave. It is important to distinguish between the influence of karst architecture and climate-driven processes, such as drought, on discharge

581 so that paleoclimate proxy records from associated speleothems can be appropriately
582 constrained. This study has increased our understanding of karst architecture, information
583 which can be utilised in proxy-system models or forward models, approaches that are
584 increasingly used to understand cave drip rate variability and to model speleothem proxies
585 such as $\delta^{18}O$ (Bradley et al., 2010; Cuthbert et al., 2014a). Additionally, we propose that an
586 important part of any protocol for inferring karst architecture is 1) the incorporation of cave
587 drip rate monitoring with a minimum 15 min interval at multiple discharge sites for at least a
588 year and 2) the systematic investigation of daily, weekly and monthly timescales using
589 frequency analysis capable of showing frequency-time changes, such as the synchrosqueeze
590 transform (Daubechies et al., 2011) to infer karst flow processes and their relative
591 importance. This study clearly demonstrates the potential for vegetation to impact karst
592 water recharge making this research relevant to karst modelling and karst water resources
593 assessment. Currently, there are no approaches that consider the impacts of vegetation on
594 recharge dynamics in process-based karst models (Hartmann et al., 2014b, 2015) or in
595 empirical recharge estimation approaches (Allocca et al., 2014; Andreo et al., 2006).

596 This is the first volumetric observation of tree water use in cave drip water. This supports a
597 growing number of studies examining the impact of trees on karst processes and
598 paleoclimate proxies. For example, tree root respiration provides a source of CO_2 for the
599 dissolution of limestone that is additional to that from soil and vadose zone microbial
600 respiration. Coleborn et al (2016) found that vegetation regeneration determined post-fire
601 soil CO_2 in a study investigating post-fire impacts on karst processes. Direct observations of
602 tree water use within the karst unsaturated zone implies the presence of root respiration, a
603 process which in turn affects drip water and speleothem ^{14}C and $\delta^{13}C$ composition (Fairchild
604 and Baker, 2012; Meyer et al., 2014; Noronha et al., 2015). Trees have been demonstrated
605 to have long-term effects on cave drip-water solute concentrations. Treble et al. (2015,
606 submitted) demonstrate long-term trends in drip water calcium and trace element
607 concentration, which they attribute to increasing solute concentration due to forest
608 regrowth and increased post-fire tree water use. Baldini et al (2005) infer an effect on
609 speleothem $\delta^{18}O$ due to secondary forest regrowth after mining and Wong and Banner
610 (2010) found clearing surface vegetation changed drip water Mg/Ca and Sr/Ca. The findings
611 and suggested protocol in this study will inform the selection of speleothem specimens for
612 further research into the impact of tree water use on speleothem paleoclimate proxies.

613 **5. Conclusions**
614

615 We demonstrated a novel method of analysing recurring patterns in cave water drip rate
616 using the synchrosqueezing transform (SST). Our analysis revealed daily and sub-daily
617 oscillations with variable temporal and spatial signatures. We tested competing hypotheses
618 for causes of daily oscillations using drip rate, barometric and temperature data. The only
619 hypothesis which all the data and hydrologic theory were consistent, was that daily

fluctuations in drip rate were driven by tree water use. We proposed that the complexity of flow pathways in the karst system accounted for the spatial and temporal variation in the daily fluctuations of drip rate. This was explored in detail using conceptual models. The results have wider implications for karst research including providing a new protocol for inferring karst architecture, informing selection of speleothem specimens for tree water use paleoclimate studies and highlighting the importance of vegetation dynamics on karst recharge.

Author contribution

KC, MOC, GCR and AB wrote the manuscript, discussed the results and implications and commented on the manuscript at all stages. KC, AB and ON collected data. GCR performed the SST analysis and generated the SST figures. GCR and ON created the location map. KC generated other graphs and conceptual figures.

Acknowledgements

We acknowledge that Katie Coleborn was supported the Australian Research Council (LP130100177). Mark Cuthbert was supported by Marie Curie Research Fellowship funding from the European Community's Seventh Framework Programme [FP7/2007-2013] under grant agreement n.299091. We would also like to thank Stuart Hankin for allowing us access to the weather station data and the National Parks and Wildlife Service staff at Yarrangobilly Caves. Solar exposure data derived from satellite imagery processed by the Bureau of Meteorology from the Geostationary Meteorological Satellite and MTSAT series operated by Japan Meteorological Agency and from GOES-9 operated by the National Oceanographic & Atmospheric Administration (NOAA) for the Japan Meteorological Agency. We would also like to acknowledge the use of equipment funded by the Australian Government National Collaborative Research Infrastructure Strategy (NCRIS).

References

Acworth, R. I., Rau, G. C., McCallum, A. M., Andersen, M. S. and Cuthbert, M. O.: Understanding connected surface-water/groundwater systems using Fourier analysis of daily and sub-daily head fluctuations, Hydrogeol. J., 23(1), 143–159, doi:10.1007/s10040-014-1182-5, 2015.

Adamson, L. and Loudon, A.: Wagga Geological Sheet, SI/55-15, 1st edition, 1:250000, 1966.

Allocca, V., Manna, F. and De Vita, P.: Estimating annual groundwater recharge coefficient for karst aquifers of the southern Apennines (Italy), Hydrol. Earth Syst. Sci., 18(2), 803–817, doi:10.5194/hess-18-803-2014, 2014.

Andreo, B., Vias, J., Duran, J. J. and Jimenez, P.: Methodology for groundwater recharge assessment in carbonate aquifers: application to pilot sites in southern Spain, Hydrogeol. J.,

16, 911–925, 2006.

Arbel, Y., Greenbaum, N., Lange, J. and Inbar, M.: Infiltration processes and flow rates in developed karst vadose zone using tracers in cave drips, Earth Surf. Process. Landforms, 35(14), 1682–1693, doi:10.1002/esp.2010, 2010.

Auger, F. and Flandrin, P.: Improving the readability of time-frequency and time-scale representations by the reassignment method, IEEE Trans. Signal Process., 43(5), 1068–1089, doi:10.1109/78.382394, 1995.

Baker, a., Bradley, C., Phipps, S. J., Fischer, M., Fairchild, I. J., Fuller, L., Spötl, C. and Azcurra, C.: Millennial-length forward models and pseudoproxies of stalagmite $\delta^{18}O$: an example from NW Scotland, Clim. Past, 8(4), 1153–1167, doi:10.5194/cp-8-1153-2012, 2012.

Baker, A. and Brunsdon, C.: Non-linearities in drip water hydrology: an example from Stump Cross Caverns, Yorkshire, J. Hydrol., 277(3-4), 151–163, doi:10.1016/S0022-1694(03)00063-5, 2003.

Baldini, J. U. L., McDermott, F., Baker, a, Baldini, L. M., Mattey, D. P. and Railsback, L. B.: Biomass effects on stalagmite growth and isotope ratios: A 20th century analogue from Wiltshire, England, Earth Planet. Sci. Lett., 240(2), 486–494, doi:10.1016/j.epsl.2005.09.022, 2005.

Baldini, J. U. L., McDermott, F., Baldini, L. M., Ottley, C. J., Linge, K. L., Clipson, N. and Jarvis, K. E.: Identifying short-term and seasonal trends in cave drip water trace element concentrations based on a daily-scale automatically collected drip water dataset, Chem. Geol., 330-331, 1–16, doi:10.1016/j.chemgeo.2012.08.009, 2012.

Bradley, C., Baker, A., Jex, C. N. and Leng, M. J.: Hydrological uncertainties in the modelling of cave drip-water δ18O and the implications for stalagmite palaeoclimate reconstructions, Quat. Sci. Rev., 29(17-18), 2201–2214, doi:10.1016/j.quascirev.2010.05.017, 2010.

Burgess, S. S. O., Adams, M. a., Turner, N. C., White, D. a. and Ong, C. K.: Tree roots: Conduits for deep recharge of soil water, Oecologia, 126(2), 158–165, doi:10.1007/s004420000501, 2001.

Carbon, B. A., Bartle, G. A., Murray, A. M. and Macpherson, D. K.: The distribution of root length, and the limits to flow of soil water to roots in a dry sclerophyll forest, For. Sci., 26(4), 656–664, 1980.

Collister, C. and Mattey, D.: Controls on water drop volume at speleothem drip sites: An experimental study, J. Hydrol., 358, 259–267, doi:10.1016/j.jhydrol.2008.06.008, 2008.

Crombie, D. S.: Root depth, leaf area and daytime water relations of Jarrah (Eucalyptus marginata) forest overstorey and understorey during summer drought, Aust. J. Bot., 40(1988), 113–22, doi:10.1071/BT9920113, 1992.

Cuthbert, M., Baker, A., Jex, C., Graham, P., Treble, P., Andersen, M. and Acworth, I.: Drip water isotopes in semi-arid karst: Implications for speleothem paleoclimatology, Earth Planet. Sci. Lett., 395, 194–204, doi:10.1016/j.epsl.2014.03.034, 2014a.

694 Cuthbert, M. O., Rau, G. C., Andersen, M. S., Roshan, H., Rutlidge, H., Marjo, C. E.,
695 Markowska, M., Jex, C. N., Graham, P. W., Mariethoz, G., Acworth, R. I. and Baker, a:
696 Evaporative cooling of speleothem drip water., Sci. Rep., 4, 5162, doi:10.1038/srep05162,
697 2014b.

698 Daubechies, I., Lu, J. and Wu, H. T.: Synchrosqueezed wavelet transforms: An empirical
699 mode decomposition-like tool, Appl. Comput. Harmon. Anal., 30(2), 243–261,
700 doi:10.1016/j.acha.2010.08.002, 2011.

701 Dawson, T. E. and Pate, J. S.: Seasonal water uptake and movement in root systems of
702 Australian phraeatophytic plants of dimorphic root morphology: a stable isotope
703 investigation, Oecologia, 107(1), 13–20, doi:10.1007/BF00582230, 1996.

704 Fairchild, I. J. and Baker, A.: Speleothem Science: From Process to Past Environments, 1st
705 ed., Wiley-Blackwell., 2012.

706 Fairchild, I. J., Borsato, A., Tooth, A. F., Frisia, S., Hawkesworth, C. J., Huang, Y. and
707 Mcdermott, F.: Controls on trace element ž Sr – Mg / compositions of carbonate cave
708 waters : implications for speleothem climatic records, 2000.

709 Farrington, P., Turner, J. and Gailitis, V.: Eucalyptus marginata, Trees, 11, 9–15, 1996.

710 Ford D. and P. D. Williams (1994) Karst Hydrogeology and Geomorphology, Wiley,
711 Chichester.

712 Genty, D. and Deflandre, G.: Drip flow variations under a stalactite of the Pere Noel cave
713 (Belgium). Evidence of seasonal variations and air pressure constraints, J. Hydrol., 211(1-4),
714 208–232, doi:10.1016/S0022-1694(98)00235-2, 1998.

715 Gribovszki, Z., Szilágyi, J. and Kalicz, P.: Diurnal fluctuations in shallow groundwater levels
716 and streamflow rates and their interpretation - A review, J. Hydrol., 385(1-4), 371–383,
717 doi:10.1016/j.jhydrol.2010.02.001, 2010.

718 Hartmann, a, Goldscheider, N., Wagener, T., Lange, J. and Weiler, M.: Karst water resources
719 in a changing world: Approaches, of hydrological modeling, Rev. Geophys., (1), 1–25,
720 doi:10.1002/2013RG000443.Received, 2014a.

721 Hartmann, A., Mudarra, M., Andreo, B., Marin, A., Wagener, T. and Lange, J.: Modelling
722 spatiotemporal impacts of hydroclimatic extremeson groundwater recharge at a
723 Mediterranean karst aquifer, Water Resour. Res., 50, 6507–6521,
724 doi:10.1002/2014WR015685.Received, 2014b.

725 Hartmann, A., Gleeson, T., Rosolem, R., Pianosi, F., Wada, Y. and Wagener, T.: A large-scale
726 simulation model to assess karstic groundwater recharge over Europe and the
727 Mediterranean, Geosci. Model Dev., 8(6), 1729–1746, doi:10.5194/gmd-8-1729-2015, 2015.

728 Hu, C., Henderson, G. M., Huang, J., Chen, Z. and Johnson, K. R.: Report of a three-year
729 monitoring programme at Heshang Cave, Central China, Int. J. Speleol., 37(October), 143–
730 151, doi:10.5038/1827-806X.37.3.1, 2008.

731 Jex, C. N., Mariethoz, G., Baker, A., Graham, P., Andersen, M. S., Acworth, I., Edwards, N.

732 and Azcurra, C.: Spatially dense drip hydrological monitoring and infiltration behaviour at
733 the Wellington Caves, South East Australia, Int. J. Speleol., 41(2), 283–296, 2012.

734 Lange, J., Arbel, Y., Grodek, T. and Greenbaum, N.: Water percolation process studies in a
735 Mediterranean karst area, Hydrol. Process., 24(13), 1866–1879, doi:10.1002/hyp.7624,
736 2010.

737 Mahmud, K., Mariethoz, G., Baker, a., Treble, P. C., Markowska, M. and McGuire, E.:
738 Estimation of deep infiltration in unsaturated limestone environments using cave LiDAR and
739 drip count data, Hydrol. Earth Syst. Sci. Discuss., 12(9), 8891–8925, doi:10.5194/hessd-12-
740 8891-2015, 2015.

741 Mariethoz, G., Baker, A., Sivakumar, B., Hartland, A. and Graham, P.: Chaos and irregularity
742 in karst percolation, Geophys. Res. Lett., 39(23), n/a–n/a, doi:10.1029/2012GL054270, 2012.

743 Markowska, M., Baker, A., Treble, P. C., Andersen, M. S., Hankin, S., Jex, C. N., Tadros, C. V.
744 and Roach, R.: Unsaturated zone hydrology and cave drip discharge water response:
745 Implications for speleothem paleoclimate record variability, J. Hydrol.,
746 doi:10.1016/j.jhydrol.2014.12.044, 2015.

747 McDonald, J.: The 2002–2003 El Niño recorded in Australian cave drip waters: Implications
748 for reconstructing rainfall histories using stalagmites, Geophys. Res. Lett., 31(22),
749 doi:10.1029/2004GL020859, 2004.

750 McDonald, J. and Drysdale, R.: Hydrology of cave drip waters at varying bedrock depths
751 from a karst system in southeastern Australia, Hydrol. Process., 1748(March), 1737–1748,
752 doi:10.1002/hyp, 2007.

753 Merritt, M. L.: Estimating Hydraulic Properties of the Floridan Aquifer System by Analysis of
754 Effects , Collier and Hendry Counties , Florida, Secretary, 70, 2004.

755 Meyer, K. W., Feng, W., Breecker, D. O., Banner, J. L. and Guilfoyle, A.: Interpretation of
756 speleothem calcite δ13C variations: Evidence from monitoring soil CO2, drip water, and
757 modern speleothem calcite in central Texas, Geochim. Cosmochim. Acta, 142, 281–298,
758 doi:10.1016/j.gca.2014.07.027, 2014.

759 Noronha, A. L., Johnson, K. R., Southon, J. R., Hu, C., Ruan, J. and McCabe-Glynn, S.:
760 Radiocarbon evidence for decomposition of aged organic matter in the vadose zone as the
761 main source of speleothem carbon, Quat. Sci. Rev., 127, 37–47,
762 doi:10.1016/j.quascirev.2015.05.021, 2015.

763 Peel, M. C., Finlayson, B. L. and Mcmahon, T. a: Updated world map of the K oppen-Geiger
764 climate classification, Hydrol. Earth Syst. Sci. Discuss., 4, pp. 439–473, doi:10.5194/hess-11-
765 1633-2007, 2007.

766 Proctor, C. J., Baker, a., Barnes, W. L. and Gilmour, M. a.: A thousand year speleothem
767 proxy record of North Atlantic climate from Scotland, Clim. Dyn., 16(10-11), 815–820,
768 doi:10.1007/s003820000077, 2000.

769 Rau, G. C., Cuthbert, M. O., Andersen, M. S., Baker, A., Rutlidge, H., Markowska, M., Roshan,
770 H., Marjo, C. E., Graham, P. W. and Acworth, R. I.: Controls on cave drip water temperature

771 and implications for speleothem-based paleoclimate reconstructions, Quat. Sci. Rev., 127,
772 1–18, doi:10.1016/j.quascirev.2015.03.026, 2015.

773 Rutlidge, H., Baker, A., Marjo, C. E., Andersen, M. S., Graham, P. W., Cuthbert, M. O., Rau, G.
774 C., Roshan, H., Markowska, M., Mariethoz, G. and Jex, C. N.: Dripwater organic matter and
775 trace element geochemistry in a semi-arid karst environment: Implications for speleothem
776 paleoclimatology, Geochim. Cosmochim. Acta, 135, 217–230,
777 doi:10.1016/j.gca.2014.03.036, 2014.

778 Sheffer, N. a., Cohen, M., Morin, E., Grodek, T., Gimburg, A., Magal, E., Gvirtzman, H., Nied,
779 M., Isele, D. and Frumkin, A.: Integrated cave drip monitoring for epikarst recharge
780 estimation in a dry Mediterranean area, Sif Cave, Israel, Hydrol. Process., 25(18), 2837–
781 2845, doi:10.1002/hyp.8046, 2011.

782 Sondag, F., Van Ruymbeke, M., Soubiès, F., Santos, R., Somerhausen, A., Seidel, A. and
783 Boggiani, P.: Monitoring present day climatic conditions in tropical caves using an
784 Environmental Data Acquisition System (EDAS), J. Hydrol., 273(1-4), 103–118,
785 doi:10.1016/S0022-1694(02)00362-1, 2003.

786 Spate, A.: Karst Values, Hurstville., 2002.

787 Stern, H., Hoedt, G. de and Ernst, J.: Objective classification of Australian Climates, Bur.
788 Meteorol. [online] Available from:
789 http://www.bom.gov.au/climate/environ/other/koppen_explain.shtml (Accessed 15
790 October 2013), 2012.

791 Thakur, G., Brevdo, E., Fučkar, N. S. and Wu, H. T.: The Synchrosqueezing algorithm for time-
792 varying spectral analysis: Robustness properties and new paleoclimate applications, Signal
793 Processing, 93(5), 1079–1094, doi:10.1016/j.sigpro.2012.11.029, 2013.

794 Tooth, A. F. and Fairchild, I. J.: Soil and karst aquifer hydrological controls on the
795 geochemical evolution of speleothem-forming drip waters, Crag Cave, southwest Ireland, J.
796 Hydrol., 273(1-4), 51–68, doi:10.1016/S0022-1694(02)00349-9, 2003.

797 Treble, P., Markowska, M., Tadros, C., Jex, C., Coleborn, K., Dredge, J., Baker, A., Roach, R.
798 and Spate, A.: Reconstructing past environmental change at Yarrangobilly Caves, pp. 83–88.,
799 2013a.

800 Treble, P. C., Bradley, C., Wood, A., Baker, A., Jex, C. N., Fairchild, I. J., Gagan, M. K., Cowley,
801 J. and Azcurra, C.: An isotopic and modelling study of flow paths and storage in Quaternary
802 calcarenite, SW Australia: implications for speleothem paleoclimate records, Quat. Sci. Rev.,
803 64, 90–103, doi:10.1016/j.quascirev.2012.12.015, 2013b.

804 Treble, P. C., Fairchild, I. J., Griffiths, A., Baker, A., Meredith, K. T., Wood, A. and McGuire, E.:
805 Impacts of cave air ventilation and in-cave prior calcite precipitation on Golgotha Cave
806 dripwater chemistry, southwest Australia, Quat. Sci. Rev., 127,
807 doi:10.1016/j.quascirev.2015.06.001, 2015.

808 Treble, P. C., Fairchild, I. J., Baker, A., Meredith, K. M., Andersen, M. S., Salmon, S. U.,
809 Bradley, C., Wynn, P. M., Hankin, S., Wood, A. and McGuire, E.: Roles of bioproductivity,
810 transpiration and fire in an eight-year record of cave dripwater chemistry from a forested

811 catchment, southwest Australia, 2016.

812 Tremaine, D. M. and Froelich, P. N.: Speleothem trace element signatures: A hydrologic
813 geochemical study of modern cave dripwaters and farmed calcite, Geochim. Cosmochim.
814 Acta, 121, 522–545, doi:10.1016/j.gca.2013.07.026, 2013.

815 Webb, M., Dredge, J., Barker, P. A., M??ller, W., Jex, C., Desmarchelier, J., Hellstrom, J. and
816 Wynn, P. M.: Quaternary climatic instability in south-east Australia from a multi-proxy
817 speleothem record, J. Quat. Sci., 29(6), 589–596, doi:10.1002/jqs.2734, 2014.

818 Wong, C. and Banner, J. L.: Response of cave air CO2 and drip water to brush clearing in
819 central Texas: Implications for recharge and soil CO2 dynamics, J. Geophys. Res., 115,
820 doi:10.1029/2010JG001301, 2010.

821 Worboys, G.: Koscuisko National Park Geology and Geomorphology, National Parks and
822 Wildlife Services, Sydney., 1982.

823 Zapater, M., Hossann, C., Bréda, N., Bréchet, C., Bonal, D. and Granier, A.: Evidence of
824 hydraulic lift in a young beech and oak mixed forest using 18O soil water
825 labelling, Trees - Struct. Funct., 25(5), 885–894, doi:10.1007/s00468-011-0563-9, 2011.

826